

# Detection of subsidence in Bad Frankenhausen with time series analysis of interferometric Radar

ROBERT SCHUMANN, M.Sc., DR. SANAZ VAJEDIAN

The area of Bad Frankenhausen, a small city in Thuringia in central Germany is subject to land subsidence because of the occurrence of sinkholes. We use SAR interferometry (InSAR) time series analysis to monitor the subsidence in this area. All the available C-band Sentinel-1A data in both geometries of ascending and descending are collected in this study. We exploit Small Baseline Subset (SBAS) as a time series algorithm to derive the subsidence rate of the study area. The accuracy of the SBAS time series analysis could be affected by high rate of atmospheric artifacts especially over the humid area, therefore, selection of the appropriate method of the atmospheric correction is required. In this study, a statistical based atmospheric correction method is performed to decrease the atmospheric influence. The time series analysis result in both geometries show a low rate of deformation signal along LOS directions with nearly negative sign corresponding subsidence phenomena. Availability of the InSAR time series results in both ascending and descending tracks enables us to estimate the horizontal and vertical displacement using the decomposition process. The results show a very small rate of movement, almost zero, along with horizontal direction. Vertical displacements with a maximum subsidence rate of  $1.4 \text{ mm} \cdot \text{a}^{-1}$  are observed over the area. The results of the time series analysis are partially compared to GNSS and leveling data.

**Keywords** – InSAR, subsidence, time series analysis, Sentinel-1

## 1. Introduction

Active remote sensing with synthetic aperture radar technology does not only provide spatial information of the surface of the Earth. Radar interferometry is a sophisticated imaging technique to survey and map the topography of the Earth as well as the change over time. By exploiting the phase information of the radar signal, interferometry can indicate subsidence. This technique can be largely improved by using a time series analysis (WOODHOUSE, 2005).

We use Small Baseline Subset (SBAS) InSAR time series analysis to estimate the ongoing deformation in areas prone to sinkhole formation. All the available SAR data acquired from Sentinel-1, spanning 2014 to 2018, are collected to produce subsidence velocity maps. The processing is started with constructing the initial SBAS networks includes all the pairs that have temporal and perpendicular baseline less than a defined threshold. The Differential InSAR technique (DInSAR) is then applied on the selected pairs to remove the topographic phase component and resolves the interferometric phase contribution due to the deformation. The DInSAR processing starts with coregistration process and follows by interferogram generation, flat earth and topography phase removal, filtering and unwrapping analysis. The unwrapped phase is finally entered to SBAS analysis to extract the time series maps over the area.

### 1.1. Radar Basics

Radar uses microwaves in a frequency band from about 1 *cm* up to 30 *cm*. An Antenna creates such a microwave pulse which is then backscattered by the surface of the Earth. The half of the two-way-traveltime  $\Delta t$  times the propagation speed of the signal  $c$  gives the distance  $D$  between the platform and the Earth:

$$D = \frac{\Delta t c}{2} \quad (1)$$

Especially with spaceborne imaging radar, the footprint can be very large (up to several kilometres). To distinguish the backscattered signals, a side looking antenna is always used. Using Pulse compression methods, a high resolution in the range direction can be achieved. Gaining a higher resolution in the direction of the satellite movement (azimuth) is more challenging (WOODHOUSE 2005, RICHARDS 2009).

### 1.2. SAR - Synthetic aperture radar

The resolution in azimuth direction  $\alpha$  depends on the used wavelength of the microwave carrier wave  $\lambda$  and the diameter or aperture of the antenna  $A$ :

$$\alpha = \frac{\lambda}{D} \quad (2)$$

Taking for granted this principle, achieving centimeter precision in azimuth direction should not be possible. One main goal of radar is the complex representation of the measurements. Unlike optical imaging, radar consists of amplitude and phase information. The deviation of the phase value  $\psi(x)$  from the antenna to the closest point on the surface  $R_0$  let us distinguish the radar signal also in azimuth direction  $x$ :

$$\psi(x) = \frac{2\pi x^2}{\lambda R_0} \quad (3)$$

This can be geometrically interpreted by a horizontal stacking of the antenna by moving the platform thus giving a synthetical elongation of the aperture. 2D spatial information are the result of this SAR technique, so radar delivers amplitude images of the surface and phase information for every pixel (WOODHOUSE 2005, RICHARDS 2009, ROSEN 2014).

### 1.3. Radar Interferometry

SAR data are complex-valued. The phase information of one image are chaotic and seem to deliver no further information about the Earths surface. When the same place is measured twice by a repeat-pass orbit satellite, a combination of both the complex information  $B_1(x, y)$  and  $B_2(x, y)$  gives the interferogramm  $I(x, y)$ , shown in figure 1:

$$I(x, y) = B_1(x, y)B_2^*(x, y) \quad (4)$$

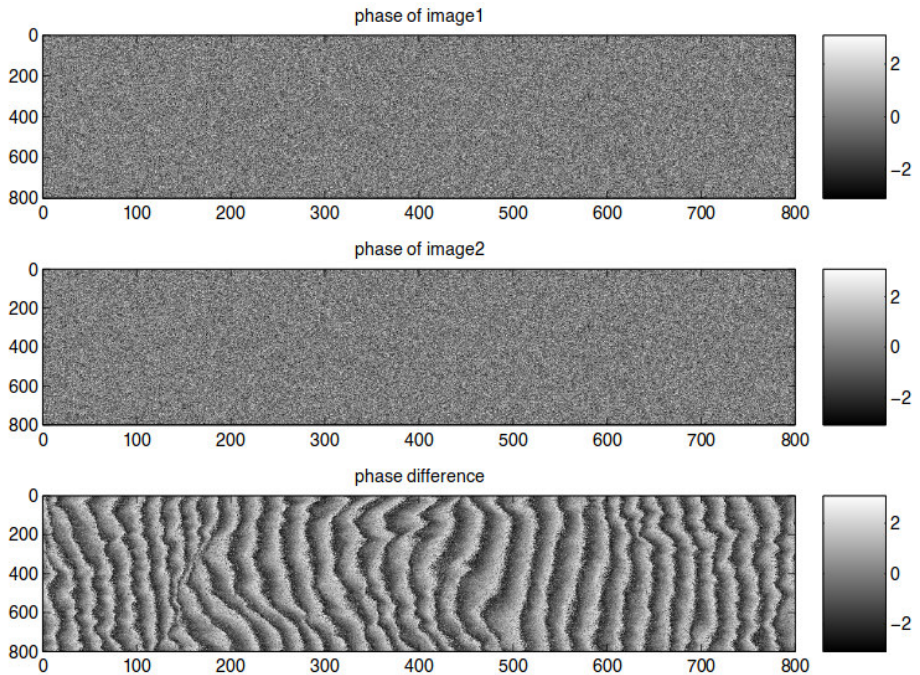


**Figure 1:** The phase information from two dates of measurement create a interferogram pattern and provide information of surface movement.

The wanted deformation information lies within the pattern of the interferogram, but several other phenomena cause a shift in the phase. Radar information has its geometrical limits because of the critical baseline. If the distance between the two platform positions is too big, one complete phase cycle will occur in less than one ground pixel  $r_g$  by a given height  $H$ :

$$B_{\perp crit} = \frac{\lambda H}{2r_g \cos(\theta)^2} \quad (5)$$

So the right choice of the interferometry pairs can be crucial (RICHARDS 2009).

### 1.3.1. Phase Unwrapping

The phase can only lie in an interval from  $[0, 2\pi]$ . This fact creates the typical pattern und wrapped interferograms like in figure 1. The after reaching the limit of this given interval the phase jumps back, so it has to be unwrapped for further processing (RICHARDS 2009, ROSEN 2014).

### 1.3.2. Errors in the interferogram

The topography as well as the flat earth without any hills or valleys can be seen in the interferogram, so they have to be removed with a digital elevation model (DEM). But still, a handful of errors remain, so the interferometric phase  $F(\psi)$  consists of:

$$F(\phi) = F \{ \phi_{def} + \phi_{atm} + \Delta\phi_{orb} + \Delta\phi_{\theta} + \phi_N \} \quad (6)$$

Because of the atmospheric influence from the ionosphere and the troposphere, a additional phase shift  $\phi_{atm}$  is caused.  $\Delta\phi_{orb}$  equals the residual phase caused by the orbit error and  $\Delta\phi_{\theta}$  is derived by errors in the DEM. Thermal noise is expressed as  $\phi_N$ . In a optimal case (two reflectors standing next to each other with a very high coherence) an accuracy of up to 1 mm can be reached in deformation analysis using spaceborne radar interferometry. This technique is called Differential interferometric SAR (DInSAR) (WOODHOUSE 2005, HOOPER ET AL. 2011).

### 1.3.3. Coherence

Coherence is a measure of the similarity of two wavefronts. In radar interferometry, the correlation between two images from different acquisition dates can be computed from this value and express the information continuity between the images (WOODHOUSE, 2005).

### 1.4. Time series analysis

For the long time monitoring of an area with several image acquisition dates using time series analysis is crucial. There are two main approaches: Persistent scatter interferometry (PSI) and the Small Baseline subset (SBAS). PSI is a single-master-technique, so only one main interferogram acts as the reference set. This has advantages in areas with a high coherence or a great backscatterer. SBAS on the other hand is a stacking method and builds up a multi-master image network, which mathematical model is similar to a levelling network.

## 2. Methodology

In this work, radar data from Sentinel-1A was used to monitor deformations in Bad Frankenhausen in Thuringia. The basical workflow for the radar interferometry and time series analysis consists of these steps:

- i. Corregistration of the image pairs using Burst overlap interferometry (BOI)
- ii. Elevation antenna pattern correction
- iii. Compute Interferograms
- iv. Flat-Earth correction and topographic correction
- v. Phase unwrapping
- vi. Correction of the atmospheric influence
- vii. Time series analysis
- viii. Decomposition in DInSAR

## 2.1. Image Coregistration

The Images from Sentinel-1A are divided in three subswaths which are also divided into nine Bursts. Because of errors in the steering of the antenna or orbital errors, the bursts do overlap which causes strong decorrelations in the overlapping areas. Using the DEM, the bursts can be stitched together and the radar images can be coregistered for the interferometry (SANDWELL ET AL. 2016, GRANDIN 2015).

## 2.2. Correction of the atmospheric influence

The troposphere as well as the ionosphere have a influence on the microwaves from radar. Using the stacking method, this influence can be vastly eliminated. The stacking method uses the approach, that the atmospheric parameters in a network of many interferograms are the same for neighbours. Here is an example for three connected interferograms:

$$\Delta\phi_{1,2} = \phi_{1,2} + a_2 - a_1 + \delta \quad \Delta\phi_{2,3} = \phi_{2,3} + a_3 - a_2 + \delta \quad (7)$$

Next to other errors  $\delta$ , the atmospheric parameter  $a_2$  appears in both of the pairs and cancel each other out. This basic method only works, if the time between the image acquisition dates is always identical and there occur no correlations. For the practical, an approximate algorithm is used (PETER & BEKAERT 2015, TYMOFYEYeva & FIALKO 2015).

## 2.3. Time series analysis

The mathematical model for the SBAS analysis is:

$$\Delta\phi_{i,j} = (\phi_i - \phi_j) + C B_{\perp i,j} + \delta M_i \quad (8)$$

$\Delta\phi_{i,j}$  is the measured phase difference in every interferogram,  $(\phi_i - \phi_j)$  the deformation (as phase residual),  $C$  a scaling factor and  $\delta M_i$  the master error.  $B_{\perp i,j}$  is the perpendicular baseline. Besides PSI, where only one single master image exists, SBAS is a multi-master method. A master error occurs between these images. The main mathematic model for an adjustment is  $l = Ax$ .  $l$  are the observations,  $A$  is the adjustment matrix and  $x$  the final parameters, so the model here can be described as followed:

$$\begin{bmatrix} \phi_1 \\ \vdots \\ \phi_n \\ C \\ \delta M_1 \\ \vdots \\ \delta M_i \end{bmatrix} = \begin{bmatrix} 1 & \cdots & 0 & B_{\perp 1,2} & 1 & \cdots & 0 \\ 0 & \cdots & 0 & B_{\perp 1,3} & 1 & \cdots & 0 \\ \vdots & \ddots & \vdots & \vdots & \vdots & \ddots & \vdots \\ 0 & \cdots & -1 & B_{\perp i,j} & 0 & \cdots & 1 \end{bmatrix} \cdot \begin{bmatrix} \Delta\phi_{1,2} \\ \Delta\phi_{1,3} \\ \vdots \\ \Delta\phi_{i,j} \end{bmatrix} \quad (9)$$

To compute the annual speed of the deformations, the temporal distance between the image acquisition dates is used (SANDWELL ET AL. 2016, VAJEDIAN ET AL. 2015).

Spatio-temporal decorrelation is one of the issue facing the agriculture areas. In order to reduce the decorrelation effect, here we reconstruct a modified SBAS network, which only includes the interferometric pairs that are highly correlated over the study area.

#### 2.4. Decomposition in DInSar

The deformation from the descending and the ascending orbit from Sentinel-1A can be decomposed, so that there is only a height and horizontal component.

### 3. Results

Sinkholes are round or elliptical depression areas on the surface of the Earth that originate from geological processes in the underground. Three sinkholes are abundant in Bad Frankenhausen and they are monitored by the GNSS and levelling campaign SIMULTAN. Out from over 2000 interferograms from 2015-2018 two SBAS-networks were created. The network for the ascending orbit is shown in figure 2.

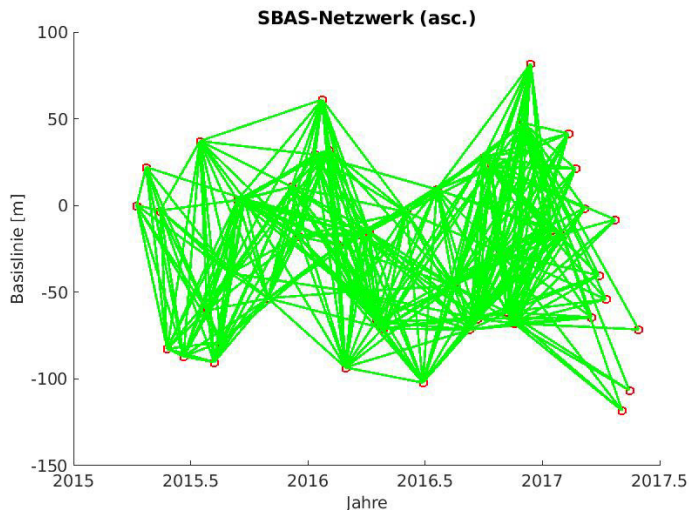


Figure 2: The SBAS network for the ascending orbit.

One for the ascending orbit and the descending orbit. Every orbit data result in two results of the displacement in range direction of the radar. They are shown in figure 3 to 5.

Using the decomposition technique, the displacement information can be used to transform both range directed maps into pure height-subsidence information:

The measurements could not be compared to the SIMULTAN study of the are, because the region around the sinkholes has a lack of coherence due to vegetation around them.

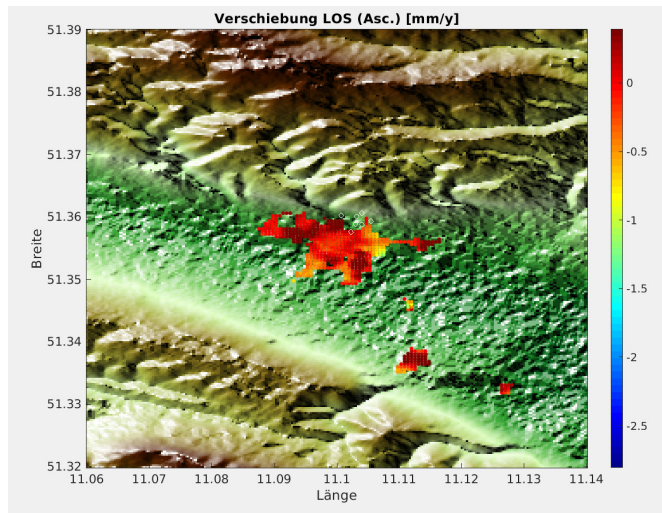


Figure 3: Result of the ascending orbit. Shown are the deformation rates in range direction. They lie mostly around  $0 \text{ mm} \cdot \text{a}^{-1}$

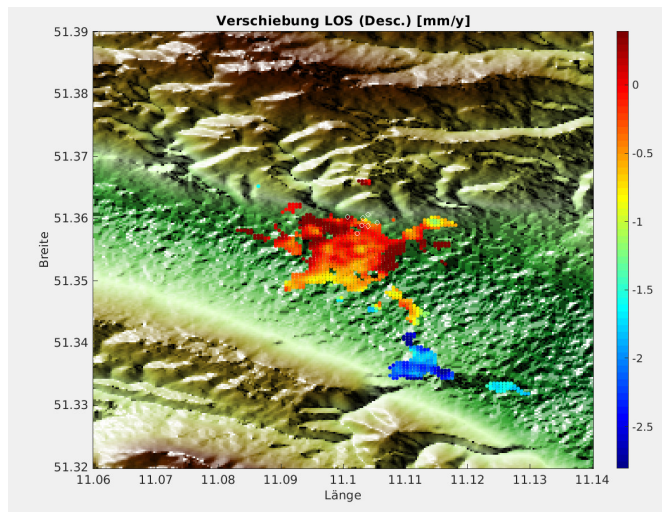


Figure 4: Result of the descending orbit. Shown are the deformation rates in range direction. They lie mostly around  $0 \text{ mm} \cdot \text{a}^{-1}$ .

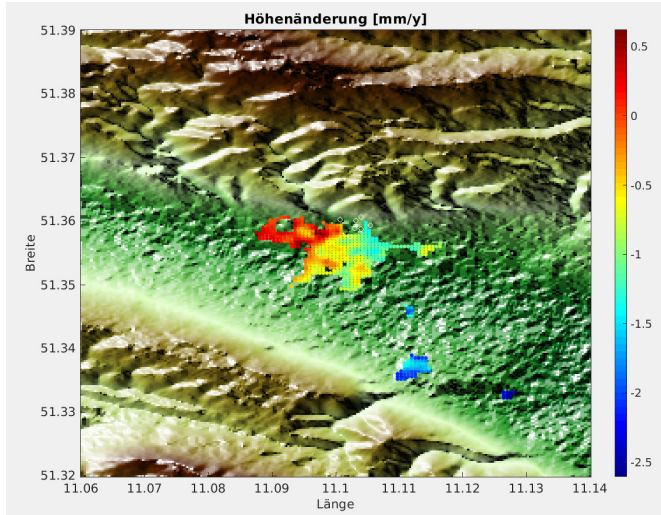


Figure 5: Result after decomposition. Shown are the subsidence rates in height. They go straight up to  $1.4 \text{ mm} \cdot \text{a}^{-1}$ .

#### 4. Discussion and conclusion

In this study we use all the available Sentinel-1 data over the area of Bad Frankenhausen, north Germany to measure the subsidence rate of the area.

One of the main issues of radar interferometry is the loss of coherence. This occurs mostly in vegetated areas like forests or on fields. Buildings in urban areas however can increase the coherence, because the backscattering remains constant. But in townparks again the coherence is often low. The results of this work do not cover the area over the three sinkholes because vegetation is abundant. But the radar data cover most of the rest of the city and this region is stable. Near to the sinkholes, a depression rate of up to  $1.4 \text{ mm} \cdot \text{a}^{-1}$  can be measured. In the rest of the city, the annual rate of subsidence is nearly  $0 \text{ mm} \cdot \text{a}^{-1}$ . This also shows, that the atmospheric influence was eliminated. Water vapour over central Europe can reach levels that are so high, that an error up to  $200 \text{ mm} \cdot \text{a}^{-1}$  can occur (PETER & BEKAERT 2015).

The radar interferometry in the region of Bad Frankenhausen shows a great advantage of this technique. Deformations are measured on a large scale and extensively, whereas levelling as well as GNSS-measurements only give results for so many points. Accuracy and precision of a field subsidence analysis can be higher with a dense and highly correlated SBAS-network than with GNSS-methods (PETER & BEKAERT 2015, KERSTEN ET AL. 2017).

#### Literatur

- WOODHOUSE, I. (2005): Introduction to Microwave Remote Sensing, Taylor Francis Ltd, Boca Raton.
- RICHARDS, J. (2009): Remote Sensing with Imaging Radar, Springer Verlag, Heidelberg.



- ROSEN, P. (2014): Principles and theory of radar interferometry.
- HOOPER, BEKAERT, A. D., SPAANS, K. & ARIKAN, M. (2011): Advances in sar interferometry time series analysis for measuring crustal deformation, Tectonophysics.
- SANDWELL, D., MELLORS, R., TONG, X., XU, X., WEI, M., & WESSEL, P. (2016): GMTSAR: An InSAR Processing System Based on Generic Mapping Tools.
- GRANDIN, R. (2015): Interferometric processing of slc sentinel-1 tops data.
- PETER, D. & BEKAERT, S. (2015): Interferometric Synthetic Aperture Radar for slow slip applications, Ph.D. thesis, Leeds.
- TYMOFYEYEVA, E. & FIALKO, Y. (2015): Mitigation of atmospheric phase delays in insar data, with application to the eastern california shear zone, Journal of Geophysical Research.
- VAJEDIAN, S., MOTAGH, M. & NILFOUROUSHAN, F. (2015): Stamps improvement for deformation analysis in mountainous regions: Implications for the damavand volcano and mosha fault in alborz, Remote Sensing.
- KERSTEN, T., KOBE, M., GABRIEL, G., TIMMEN, L., SCHÖN, S. & VOGEL, D. (2017): Geodetic monitoring of subsosion-induced subsidence processes in urban areas: Concept and status report. In: Journal of Applied Geodesy 11 (2017). Nr. 1, S. 21-29. DOI: <https://doi.org/10.1515/jag-2016-0029>.